Nanoscale

Accepted Manuscript

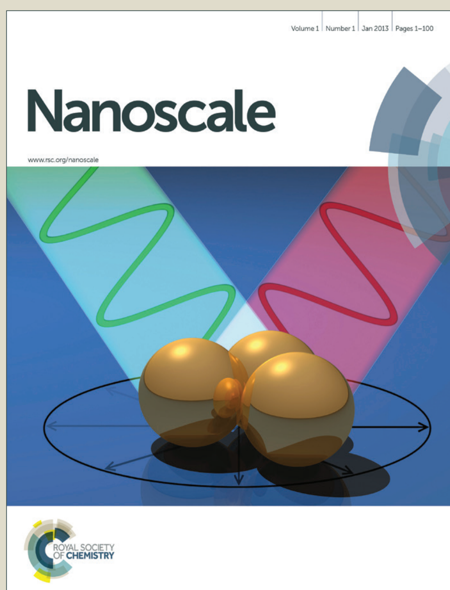

This is an *Accepted Manuscript*, which has been through the Royal Society of Chemistry peer review process and has been accepted for publication.

Accepted Manuscripts are published online shortly after acceptance, before technical editing, formatting and proof reading. Using this free service, authors can make their results available to the community, in citable form, before we publish the edited article. We will replace this *Accepted Manuscript* with the edited and formatted *Advance Article* as soon as it is available.

You can find more information about *Accepted Manuscripts* in the Information for Authors.

Please note that technical editing may introduce minor changes to the text and/or graphics, which may alter content. The journal's standard Terms & Conditions and the Ethical guidelines still apply. In no event shall the Royal Society of Chemistry be held responsible for any errors or omissions in this *Accepted Manuscript* or any consequences arising from the use of any information it contains.

ROYAL SOCIETY OF CHEMISTRY

www.rsc.org/nanoscale

Ultra-broadband and high response of the Bi_2Te_3-Si heterojunction and its application on photodetector at room temperature in harshworking environments

Jiandong Yao [a], Jianmei Shao [a], Yingxin Wang [b], Ziran Zhao [b], Guowei Yang [a]*

[a] *State Key Laboratory of Optoelectronic Materials and Technologies, Nanotechnology Research Center, School of Physics & Engineering, Sun Yat-sen University, Guangzhou 510275, Guangdong, P. R. China*

[b] *Key Laboratory of Particle & Radiation Imaging (Tsinghua University) of Ministry of Education, Department of Engineering Physics, Tsinghua University, Beijing 100084, P. R. China*

*Corresponding author: stsygw@mail.sysu.edu.cn

Nanoscale Accepted Manuscript

Abstract

Broadband photodetection is central to various technological applications including imaging, sensing and optical communications. On account of its Dirac-like surface state, Topological insulator (TI) is theoretically predicted to be promising candidate materials for broadband photodetection from the infrared to the Terahertz. Here, we report the vertically-constructed ultra-broadband photodetector based on a TI Bi_2Te_3-Si heterostructure. The device demonstrated room-temperature photodetection from ultraviolet (370.6 nm) to Terahertz (118 μm) with good reproducibility. Under bias condition, the visible responsivity reaches c.a. 1 AW^{-1} and the response time is better than 100 ms. As a self-powered photodetector, it exhibits extremely high photosensitivity approaching 7.5×10^5 cm^2/W and decent detectivity as high as 2.5×10^{11} $cm\cdot Hz^{1/2}\cdot W^{-1}$. In addition, such a prototype device without any encapsulation suffers no obvious degradation after long-time exposure to air, high-energy UV illumination and acidic treatment. In summary, we demonstrate that TI-based heterostructures hold great promise for addressing the long lasting predicament of stable room-temperature high-performance broadband photodetectors.

Keywords: topological insulator, heterostructure, ultra-broadband photodetector.

Nanoscale Accepted Manuscript

Introduction

Broadband photodetector is of great significance to numerous technological applications including imaging, sensing, optical communications and energy-harvesting.[1-4] Graphene is demonstrated to possess a broad absorption spectrum covering the ultraviolet to the far-infrared.[2, 3, 5] So far, extensive efforts have been devoted to graphene-based broadband photodetectors. However, since graphene's energy band is gapless, the hot carriers recombine very fast.[6] Besides, graphene's optical absorbance (2.3%) is very weak because it is only one monolayer in thickness.[5] These drawbacks result in poor responsivity limiting to the magnitude of mAW^{-1} for the pure-graphene photodetectors.[1-3] Various approaches have been developed to optimize the device performance. For example, an optical-antenna was exploited to improve the optical absorption and the responsivity was enhanced to 17 mA/W.[7] Later, a graphene double layer heterostructure demonstrated broadband responsivity higher than 1 A/W.[8] Most recently, graphene decorated with Bi_2Te_3 layers exhibiting pronounced responsivity of 35 A/W was developed.[9] Though tremendous progresses have been achieved, the dark current of these photodetectors are dissatisfactory on account of the absence of an intrinsic gap. This prejudices considerable practical applications such as photoswitches and imaging, which demands little energy consumption and definite on-off states. Besides, the onerous improvement processes add the complexity and degrade the practicality in device implementation. Organic photodetector is also currently the subject of intense research for broadband photodetection. Nevertheless, most of the organic materials

Nanoscale Accepted Manuscript

are relatively unstable. Consequently, organic photodetectors usually suffer degradation especially under harshworking environments.[10-12] Therefore, stable high-responsive broadband photodetector has remained an urgent but unaccomplished challenge.

Topological insulator (TI), a new phase of quantum matter, possesses an insulating gap in the bulk as well as spin-momentum-locked Dirac cones on the surfaces.[13, 14] Such metallic surface states are experimentally demonstrated to be protected by time-reversal-symmetry and robust against non-magnetic perturbation.[15, 16] Recently, Zhang *et.al.* predicted that TI's Dirac-like surface state can bring strong optical absorption, which makes it promising candidate material for high-performance broadband photodetection from the infrared to the Terahertz.[17] Shao *et al.* reported that the observed warping effect in Bi_2Te_3[15] and Bi_2Se_3[18] can further enhance the device's performance.[19] What's more, experimentally, TI exhibits exceptional high surface mobility[20] and has been demonstrated to be efficient electrodes like graphene.[21 22]

In spite of considerable theoretical and experimental efforts, few researches have successfully pursued the TI-based broadband photodetector so far. The unavailability of high quality TI film, ultrafast hot carrier recombination and inappropriateness of a gapless energy band for visible-light detection stand in the way. In fact, pulsed-laser deposition (PLD) has proven to be an effective technology to deposit high-quality polycrystalline TI Bi_2 (Te, Se)$_3$ films.[23, 24] Extensive efforts have demonstrated that they provide an attractive material platform to explore TI's intrinsic nature and

Nanoscale Accepted Manuscript

potential applications, including the weak antilocalization effect[25] and the anomalous photoelectric effect[26]. Additionally, a heterojunction is believed to be efficient in the separation of photo-generated carriers with the help of a built-in electric field.[27] Thus, it is a possible settlement to the ultrafast hot carrier recombination. Furthermore, silicon, the cornerstone of the state-of-art semiconductor industry, enjoys a band gap of 1.12 eV, making it suitable for the visible to the near-infrared photodetection. Therefore, it seems that TI and Si are complementary to each other. Enlightened by this, herein, we propose the first vertically-constructed broadband photodetector based on the Bi_2Te_3-Si heterostructure. It brings about synergistic effect of both components and lead to stable high-performance broadband photodetection.

Experimental

Pulsed laser deposition (PLD) was applied to prepare the Bi_2Te_3 film on the commercially available n-Si ($< 0.05\,\Omega\cdot\text{cm}$) substrate. The parameters of the PLD-growth progress were described in detail elsewhere.[25] Prior to loading into the growth chamber, the silicon substrate was cleaned following a standard cleaning procedure to obtain an intact surface. To remove the organic pollutants, Si wafers were firstly cleaned in acetone and ethyl ethanol, respectively. Then, they were successively immersed in piranha solution (H_2SO_4 (98%): H_2O_2 (35%) =3:1) and diluted HF (HF (40%): H_2O=1:20) to remove the inorganic contaminants. Finally, the substrates were rinsed in deionized water to remove the residue. The whole process was conducted in an ultrasonic oscillation environment. The Bi_2Te_3 film, 300 μm in

Nanoscale Accepted Manuscript

diameter and 100 nm in thickness, was grown onto the Si wafer by PLD with the help of a shadow mask. Then, Pt electrode of 80 μm in diameter and 50 nm in thickness was deposited on the top surface of the Bi_2Te_3 film by sputtering. Ag electrode of 50 nm in thickness was successively deposited on the bottom surface of Si, eventually furnishing a prototype photodetector.

Illuminations with wavelength of 370 nm, 635 nm, 1064 nm and 1550 nm were generated from the semiconductor lasers. The Terahertz illumination (118.8 μm) was generated from a Fourier transform infrared spectroscopy. The electrical characteristic of the Bi_2Te_3/Si heterojunction photodetector was evaluated using a Keithley 4200-SCS semiconductor parameter analyzer. All measurements were performed at room-temperature under ambient condition.

Results and Discussion

The structure of the device is schematically shown in Fig. 1(a). The device is composed of the PLD-grown p-type Bi_2Te_3 film (Supplementary Information S1) and commercially available n-type Si substrate ($< 0.05\ \Omega \cdot \mathrm{cm}$). The dark and illuminated I-V characteristics of the Bi_2Te_3-Si heterojunction were investigated and the results are summarized in Fig. 1(b). In detail, in darkness, a highly asymmetry I-V curve is observed, indicating excellent rectifying characteristic. The rectification ratio exceeds 5×10^3. Considering the fact that Ag (Pt) forms a relatively good ohmic contact to Si (Bi_2Te_3) (Supplementary Information S2), the observed rectifying effect can be exclusively attributed to the p-Bi_2Te_3/n-Si heterojunction. On light illumination, both

Nanoscale Accepted Manuscript

the forward and reverse currents increase due to the generation of electron-hole pairs. Since the dark current under the negative bias is several orders of magnitude lower than that of the positive one, the photosensitivity of the former is much larger than that of the latter. Therefore, the negative bias is the working bias unless otherwise stated.

Taking the visible case (635 nm) for an example, we show the photoresponse of the Bi_2Te_3-Si heterojunction photodetector in Fig. 2. The I-V curves in the negative voltage region under the illumination with a serial of powers are shown in Fig. 2(a). Obviously, the current increases as the voltage increases because it helps promote the separation and transport of photogenerated carriers. It is to be noted that the photocurrent can be tuned throughout more than 2 orders of magnitude within a small voltage range. Such wide voltage tunability is an attractive feature for variable-brightness imaging applications.[22] Fig. 2(b) plots the switching behavior of the device. Upon a periodic illumination, it exhibits good reproducibility. Further measurement demonstrates that the switching behavior is stable over 1500 s (Supplementary Information S3). Unlike other reported photodetectors,[28, 29] there is no appreciable change in the magnitude of the dark current as well as the photocurrent over all on/off cycles. Then, the response speed, defined as the time taken to rise from 10% to 90% or vice versa, was investigated. Fast rise and decay speed which is better than c.a. 100 ms was demonstrated (Supplementary Information S4). This relatively quick response speed may originate from the efficient carrier collecting due to the TI's extremely high surface carrier mobility and the quick separation of the

Nanoscale Accepted Manuscript

photogenerated carriers by the built-in electric field. To gain further insight into the device's performance, measurements are conducted to investigate the power-dependent photocurrent as shown in Fig. 2(c). Clearly, we can see that the photocurrent is linear proportional to the incident power, suggesting that the photodetector can effectively distinguish different light intensity. Besides, the responsivity extracted from Fig. 2(c) approaches c.a. 1 AW^{-1}.

Finally, the possibility for a self-powered photodetector is also developed. Compared to the bias case, a self-power device enjoys considerably smaller dark currents, which results in effective photo-switches and little energy dissipation. Fig. 2(d) describes the photovoltaic characteristics of the Bi_2Te_3-Si photodetector. As shown in the graph, on light illumination, the I-V curves cross the negative side of current axis, which means that photocurrent generates without a source-drain bias. Fig. 2(e) presents the time-dependent switching behavior without bias. The result also exhibits a good reproducibility. The responsivity calculated from Fig. 2(e) is c.a. 0.017 AW^{-1}, lower than that of the bias condition. This is due to the less efficient separation and transport of the photogenerated carriers without the help of an external voltage. However, thanks to the extremely low dark current at the magnitude of 10^{-11} A, the photosensitivity of the device approaches 7.5×10^{5} cm^{2}/W, leading to a decent detectivity of $2.5\times10^{11}\ cm\cdot Hz^{1/2}\cdot W^{-1}$.

To have an intuitive impression on the device performance of the Bi_2Te_3/Si heterojunction photodetector, the results of several reported photodetectors based on Graphene (G) /Graphene Oxide (GO) is summarized in Supplementary Information

Nanoscale Accepted Manuscript

Table S1 and S2. In general, although certain parameters may be inferior to those of some excellent devices, the overall performance of our Bi_2Te_3/Si heterojunction stands out considering all performance indexes. Further improvement of the device performance can be expected with a plasmonic structure or an array structure on account of their excellent light trapping ability.[30, 31]

Fig. 3 presents the broadband photoresponse of the Bi_2Te_3-Si heterojunction photodetector from the ultraviolet to the Terahertz. Fig. 3(a)-(d) show the switching behavior of the device under a periodic illumination with different laser wavelengths, including 370 nm, 1064 nm, 1550 nm and 118.8 μm. In all illumination cases, the device yields a significant photocurrent and exhibits definite on/off states without serious background noise. It demonstrates superiority over the graphene-base photodetectors.[9, 32, 33] Note that the Fourier transform infrared spectroscopy is equipped with another measurement system with different measurement configuration. Therefore, another device was fabricated to detect the Terahertz light and thus the dark current varies quiet a lot compared to the former three cases. Besides, the profound noise in Fig. 3(d) is not the intrinsic nature of our device. Instead, it comes from a rougher measurement system.

The working principle of the Bi_2Te_3-Si heterojunction photodetector can be explained through the schematic diagram of its energy band diagram, as illustrated in Fig. 3(e). The Fermi level of Bi_2Te_3 and Si are c.a. 4.65 and c.a. 4.24 eV, respectively.[34-36] Once the Bi_2Te_3 film is deposited onto the Si substrate, electrons of Si tend to move to the Bi_2Te_3 to keep the Fermi levels of each other in alignment,

Nanoscale Accepted Manuscript

leading to electrons accumulation in Bi_2Te_3 and holes accumulation in Si. In the thermal equilibrium, an internal electric field pointing from Si to Bi_2Te_3 is built, with the energy band of Bi_2Te_3 bending downward and that of Si bending upward. The operating mechanism of the device is described as follows. On light illumination, the corresponding optical active layer absorbs the incident photons and generates electron-hole pairs. The photogenerated carriers within one carrier mean free path are rapidly separated and then swept away by the intense built-in electric field. Finally, the photogenerated carriers are collected by the electrodes, giving rise to the generation of photocurrent in external circuit.

Notably, different portion of the TI Bi_2Te_3-Si heterojunction photodetector dominates the photoresponse under illumination with different photon energy. Generally, there are three distinct active parts, including Si, Bi_2Te_3's bulk and Bi_2Te_3's surface. For the illumination beyond the band edge of Si (1.12 eV), e.g. 635 nm, Si plays the domination role on account of the stronger absorbance originated from its greater thickness. In addition, Si enjoys a more favorable band gap for detection of photons from UV to near-infrared compared to Bi_2Te_3's bulk and surface. The response mechanism is schematically described in the step I. For the illumination beyond the band edge of Bi_2Te_3 (0.15 eV) but below that of Si (1.12 eV), e.g. 1550 nm, Si shows little absorption to the incident light since the photon does not have enough energy to excite the electrons from the conduction band to the valence band. On the other hand, the surface state density of TI Bi_2Te_3 is much less compared to that of its bulk. Therefore, the bulk state of Bi_2Te_3 dominates the photocurrent in this case.

Nanoscale Accepted Manuscript

The response mechanism is schematically described in the step II. For the illumination below the band edge of Bi_2Te_3's bulk, e.g. 118.8 μm, both of Si and TI Bi_2Te_3's bulk are blind to the incident photons. However, thanks to the gapless nature of TI Bi_2Te_3's surface state, electron-hole pairs can still generate through intraband and interband excitations. Consequently, the TI's surface state induced photocurrent generates. The response mechanism is described in the step III.

At last, stability, a crucial requirement for the widely spread application, is investigated. Generally, the performance of a photodetector might be weakened by adverse working environment. For example, dopants from the ambient environment can enter the loose organic films and react with their relatively active components, which naturally leading to device failure.[10-12] Additionally, some devices are usually decorated by various functional groups.[37, 38] However, these functional groups are innately unstable to high-energy UV illumination.[29, 39] Furthermore, the deterioration under acidic environment is also an obstacle that can't be ignored on account of the growing air pollution like acid rain. Therefore, the robustness of the device to ambient condition, high-energy UV illumination and acidic treatment is evaluated.

Firstly, the durability to oxidative degradation in ambient environment is monitored. The as-fabricated device is stored under ambient condition for a month without any encapsulation. And the performance is monitored before and after the storage, as shown in Fig. 4(a). Clearly, there is no obvious difference between the two results. One reason is that the PLD-grown Bi_2Te_3 film is highly c-axis oriented. Such films have been demonstrated to possess inert properties owing to the surface layer

Nanoscale Accepted Manuscript

atom's closed electronic shells with bonds oriented into the quintuple layer.[40] In addition, due to the topological origin of the metallic surface state, the surface oxidation merely displaces the conducting surface layer underneath an oxide layer instead of removing it. Consequently, the efficient carrier collection and transport are still preserved. Secondly, a device was exposed directly to UV light (c.a. 100 mW/cm^2) for 10 minutes and the results are summarized in Fig. 4(b). Excitingly, we can see that the result exhibits no observable changes, indicating that the device is also robust against UV illumination. Finally, the acidic-resistance test was also conducted. The sample was immersed into 10% HCl solution for six hours. Again, the response of the device to cyclical illumination remains almost the same, as depicted in Fig. 4(c). Therefore, owing to the robustness of TI's non-trivial metallic surface states and low chemical activity of both components, the TI Bi_2Te_3-Si heterojunction photodetector exhibits excellent stability under various harshworking environments.

Conclusion

In summary, the Bi_2Te_3-Si heterojunction photodetector was fabricated and the device was investigated at the bias mode and the self-powered mode, respectively. Excitingly, it demonstrated ultra-broadband photoresponse from the ultraviolet to the Terahertz at room-temperature. At the bias mode, the fabricated device exhibited a high responsivity reaching 1 AW^{-1} and a short response time better than 100 ms under 635-nm illumination with good reproducibility. As a self-power photodetector, the device showed a fast response with extremely high photosensitivity exceeding

Nanoscale Accepted Manuscript

7×10^{5} cm^{2}/W and decent detectivity at the magnitude of 2.5×10^{11} $cm\cdot Hz^{1/2}\cdot W^{-1}$. Importantly, further studies demonstrated that this prototype device without any encapsulation suffers no obvious degradation after long time exposure to ambient condition, high energy UV illumination and acidic treatment. With further optimizations, e.g. improvement of the quality of the junction and the enhancement of the optical absorption, practical devices are expected in the near future. Therefore, our work shows the broad applicability of this methodology for accessing high-performance broadband photodetectors, especially, TI-based heterostructures, at room-temperature in harshworking environments.

Acknowledgements. This work was supported by the National Natural Science Foundation of China (91233203) and the State Key Laboratory of Optoelectronic Materials and Technologies supported this work.

Nanoscale Accepted Manuscript

Reference

1. F. Xia, T. Mueller, Y. M. Lin, A. Valdes-Garcia and P. Avouris, *Nat Nanotechnol*, 2009, **4**, 839-843.

2. T. Mueller, F. Xia and P. Avouris, *Nat Photon*, 2010, **4**, 297-301.

3. N. M. Gabor, J. C. Song, Q. Ma, N. L. Nair, T. Taychatanapat, K. Watanabe, T. Taniguchi, L. S. Levitov and P. Jarillo-Herrero, *Science*, 2011, **334**, 648-652.

4. K.-T. Lin, H.-L. Chen, Y.-S. Lai and C.-C. Yu, *Nat Commun*, 2014, **5**.

5. R. R. Nair, P. Blake, A. N. Grigorenko, K. S. Novoselov, T. J. Booth, T. Stauber, N. M. R. Peres and A. K. Geim, *Science*, 2008, **320**, 1308-1308.

6. K.-J. Yee, J.-H. Kim, M. H. Jung, B. H. Hong and K.-J. Kong, *Carbon*, 2011, **49**, 4781-4785.

7. C. Chakraborty, R. Beams, K. M. Goodfellow, G. W. Wicks, L. Novotny and A. Nick Vamivakas, *Appl Phys Lett*, 2014, **105**, 241114.

8. C. H. Liu, Y. C. Chang, T. B. Norris and Z. Zhong, *Nat Nanotechnol*, 2014, **9**, 273-278.

9. H. Qiao, J. Yuan, Z. Xu, C. Chen, S. Lin, Y. Wang, J. Song, Y. Liu, Q. Khan and H. Y. Hoh, *ACS nano*, 2015.

10. P. E. Burrows, V. Bulovic, S. R. Forrest, L. S. Sapochak, D. M. McCarty and M. E. Thompson, *Appl Phys Lett*, 1994, **65**, 2922-2924.

Nanoscale Accepted Manuscript

11. L. M. Do, E. M. Han, Y. Niidome, M. Fujihira, T. Kanno, S. Yoshida, A. Maeda and A. J. Ikushima, *J Appl Phys*, 1994, **76**, 5118-5121.

12. H. Aziz, Z. Popovic, C. P. Tripp, N.-X. Hu, A.-M. Hor and G. Xu, *Appl Phys Lett*, 1998, **72**, 2642-2644.

13. M. Z. Hasan and C. L. Kane, *Rev Mod Phys*, 2010, **82**, 3045-3067.

14. X. L. Qi and S. C. Zhang, *Rev Mod Phys*, 2011, **83**, 1057-1110.

15. Z. Alpichshev, J. G. Analytis, J. H. Chu, I. R. Fisher, Y. L. Chen, Z. X. Shen, A. Fang and A. Kapitulnik, *Phys Rev Lett*, 2010, **104**.

16. T. Zhang, P. Cheng, X. Chen, J.-F. Jia, X. Ma, K. He, L. Wang, H. Zhang, X. Dai, Z. Fang, X. Xie and Q.-K. Xue, *Phys Rev Lett*, 2009, **103**.

17. X. Zhang, J. Wang and S. C. Zhang, *Phys Rev B*, 2010, **82**, 245107.

18. Y. H. Wang, D. Hsieh, D. Pilon, L. Fu, D. R. Gardner, Y. S. Lee and N. Gedik, *Phys Rev Lett*, 2011, **107**.

19. J. M. Shao, H. Li and G. W. Yang, *Nanoscale*, 2014, **6**, 3513-3517.

20. J. N. Hancock, J. L. M. van Mechelen, A. B. Kuzmenko, D. van der Marel, C. Brüne, E. G. Novik, G. V. Astakhov, H. Buhmann and L. W. Molenkamp, *Phys Rev Lett*, 2011, **107**, 136803.

21. H. Peng, W. Dang, J. Cao, Y. Chen, D. Wu, W. Zheng, H. Li, Z.-X. Shen and Z.

Nanoscale Accepted Manuscript

Liu, *Nat Chem*, 2012, **4**, 281-286.

22. X. An, F. Liu, Y. J. Jung and S. Kar, *Nano letters*, 2013, **13**, 909-916.
23. H. B. Zhang, H. L. Yu and G. W. Yang, *EPL (Europhysics Letters)*, 2011, **95**, 56002.
24. S. X. Zhang, L. Yan, J. Qi, M. Zhuo, Y. Q. Wang, R. P. Prasankumar, Q. X. Jia and S. T. Picraux, *Thin Solid Films*, 2012, **520**, 6459-6462.
25. H. B. Zhang, H. L. Yu, D. H. Bao, S. W. Li, C. X. Wang and G. W. Yang, *Phys Rev B*, 2012, **86**, 075102.
26. H. Zhang, J. Yao, J. Shao, H. Li, S. Li, D. Bao, C. Wang and G. Yang, *Scientific reports*, 2014, **4**, 5876.
27. X. Wang, C. Liow, A. Bisht, X. Liu, T. C. Sum, X. Chen and S. Li, *Adv Mater*, 2015, **27**, 2207-2214.
28. Y. Cao, J. Zhu, J. Xu, J. He, J. L. Sun, Y. Wang and Z. Zhao, *Small*, 2014, **10**, 2345-2351.
29. P. Sun, M. Zhu, K. Wang, M. Zhong, J. Wei, D. Wu, Y. Cheng and H. Zhu, *Appl Phys Lett*, 2012, **101**, 053107.
30. X. Wang, C. Liow, D. Qi, B. Zhu, W. R. Leow, H. Wang, C. Xue, X. Chen and S. Li, *Adv Mater*, 2014, **26**, 3506-3512.

Nanoscale Accepted Manuscript

31. S. Pillai, K. Catchpole, T. Trupke and M. Green, *J Appl Phys*, 2007, **101**, 093105.

32. B. Y. Zhang, T. Liu, B. Meng, X. Li, G. Liang, X. Hu and Q. J. Wang, *Nat Commun*, 2013, **4**, 1811.

33. Y. Liu, R. Cheng, L. Liao, H. Zhou, J. Bai, G. Liu, L. Liu, Y. Huang and X. Duan, *Nat Commun*, 2011, **2**, 579.

34. H.-W. Tsai, T.-H. Wang, T.-C. Chan, P.-J. Chen, C.-C. Chung, A. Yaghoubi, C.-N. Liao, E. W.-G. Diau and Y.-L. Chueh, *Nanoscale*, 2014, **6**, 7780-7785.

35. R. A. Ismail, A. Al-Naimi and A. A. Al-Ani, *Semicond Sci Tech*, 2008, **23**, 075030.

36. Y. Chen, J. Analytis, J.-H. Chu, Z. Liu, S.-K. Mo, X.-L. Qi, H. Zhang, D. Lu, X. Dai and Z. Fang, *Science*, 2009, **325**, 178-181.

37. S. Stankovich, D. A. Dikin, G. H. B. Dommett, K. M. Kohlhaas, E. J. Zimney, E. A. Stach, R. D. Piner, S. T. Nguyen and R. S. Ruoff, *Nature*, 2006, **442**, 282-286.

38. T. Takenobu, T. Kanbara, N. Akima, T. Takahashi, M. Shiraishi, K. Tsukagoshi, H. Kataura, Y. Aoyagi and Y. Iwasa, *Adv Mater*, 2005, **17**, 2430-2434.

39. C. Goo Kang, S. Kyung Lee, T. Jin Yoo, W. Park, U. Jung, J. Ahn and B. Hun Lee, *Appl Phys Lett*, 2014, **104**, 161902.

40. V. A. Golyashov, K. A. Kokh, S. V. Makarenko, K. N. Romanyuk, I. P. Prosvirin, A. V. Kalinkin, O. E. Tereshchenko, A. S. Kozhukhov, D. V. Sheglov, S. V.

Nanoscale Accepted Manuscript

Eremeev, S. D. Borisova and E. V. Chulkov, *J Appl Phys*, 2012, **112**, 113702.

Nanoscale Accepted Manuscript

Figure Captions

Figure 1. TI Bi_2Te_3-Si heterojunction photodetector. (a) Schematic diagram of the Bi_2Te_3-Si heterojunction photodetector in a two pole structure. The forward bias is defined as applying a positive bias on the Bi_2Te_3 side. (b) I-V characteristics in dark (black) and under illumination (red). Power density: 40 mW/cm^2.

Figure 2. Photoresponse of the Bi_2Te_3-Si heterojunction photodetector under 635 nm illumination. (a) I-V characteristics in dark and under illumination with a serial of powers. (b) Time-dependent switching behavior. Source-drain bias: -5 V. Power density: 40 mW/cm^2. (c) The power-dependent photocurrent. Source-drain bias: -5 V. (d) Photovoltaic characteristic with a series of illumination powers. The inset is the magnified I-V characteristic in the low power range. (e) Time-dependent switching behavior at zero bias. The data in (a), (c) and (e) are shown on logarithmic scale.

Figure 3. Ultra-broadband photoresponse of the Bi_2Te_3-Si heterojunction photodetector. The time-dependent switching behavior under illumination of (a) 370 nm, power density: 9 mW/cm^2, (b) 1064 nm, power density: 40 mW/cm^2, (c) 1550 nm, 200 mW/cm^2. (d) 118.8 μm, 1.1 W/cm^2. (e) Schematic diagram of the energy band of the Bi_2Te_3-Si heterostructure under reversed source-drain bias.

Figure 4. Stability of the Bi_2Te_3-Si heterojunction photodetector under various

Nanoscale Accepted Manuscript

harsh working environments. (a) Stored in ambient environment for a month. (b) Exposed to UV illumination for 10 mins. (c) Immersed in HCl solution for 6 hours. All of the illumination power density are 40 mW/cm^2. The curves are horizontally shifted for clarity.

Nanoscale Accepted Manuscript

Figure 1

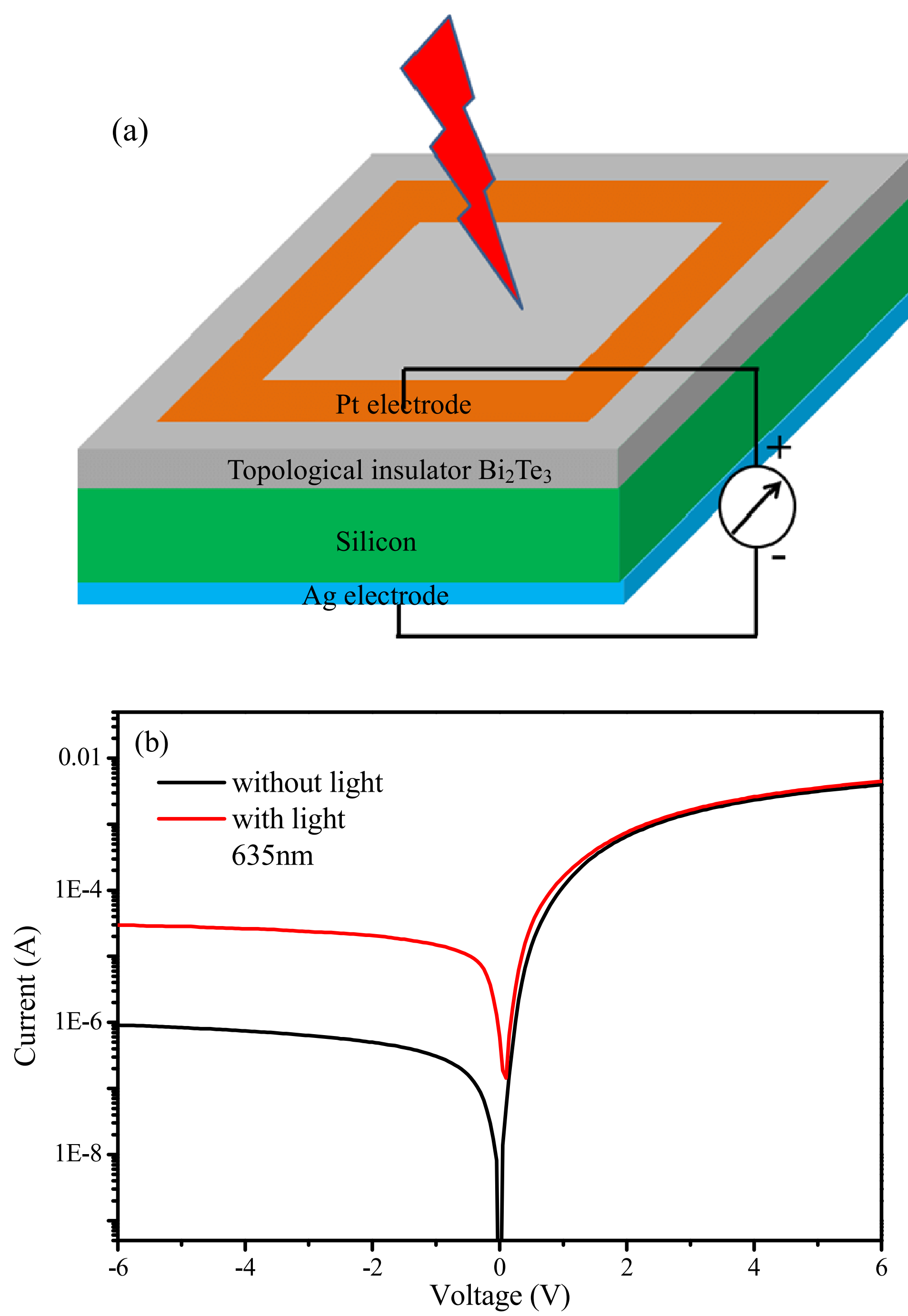

Nanoscale Accepted Manuscript

Figure 2

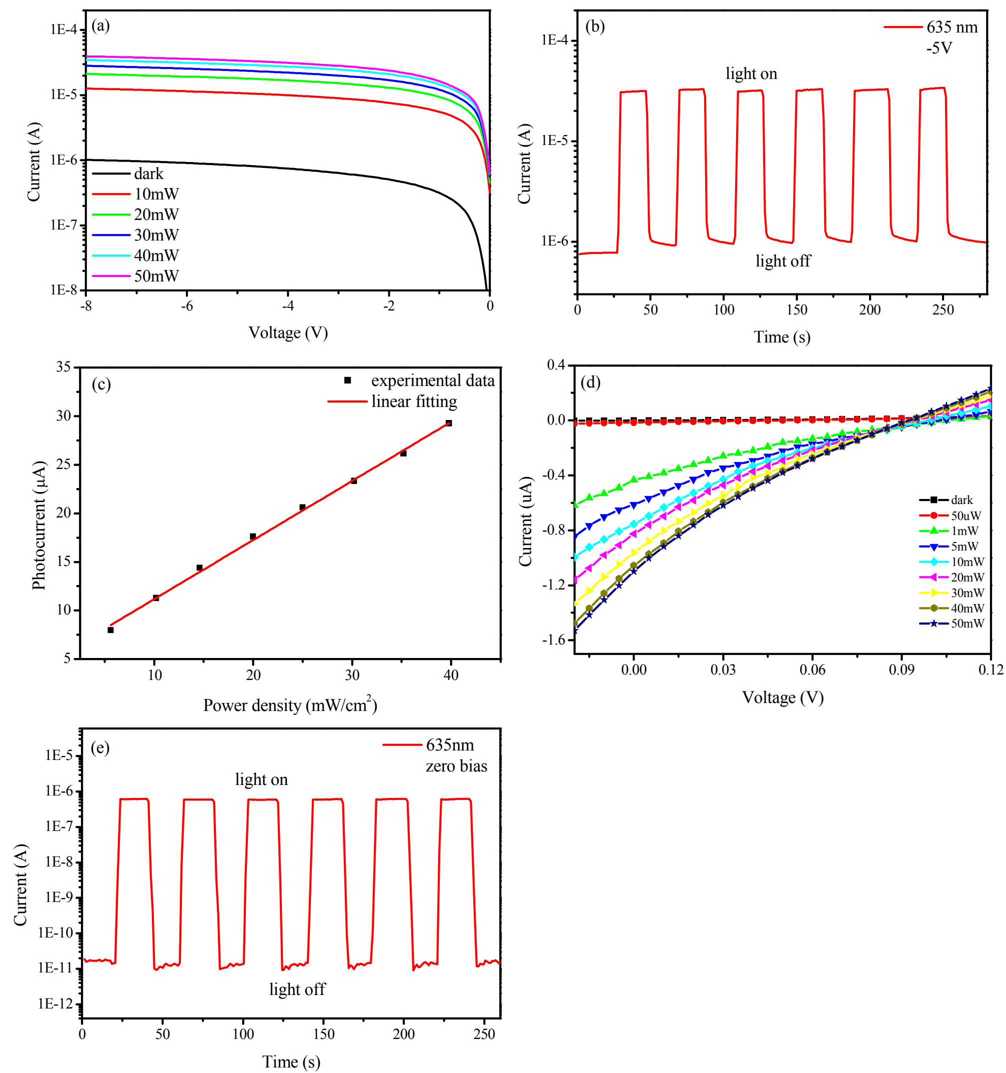

Nanoscale Accepted Manuscript

Figure 3

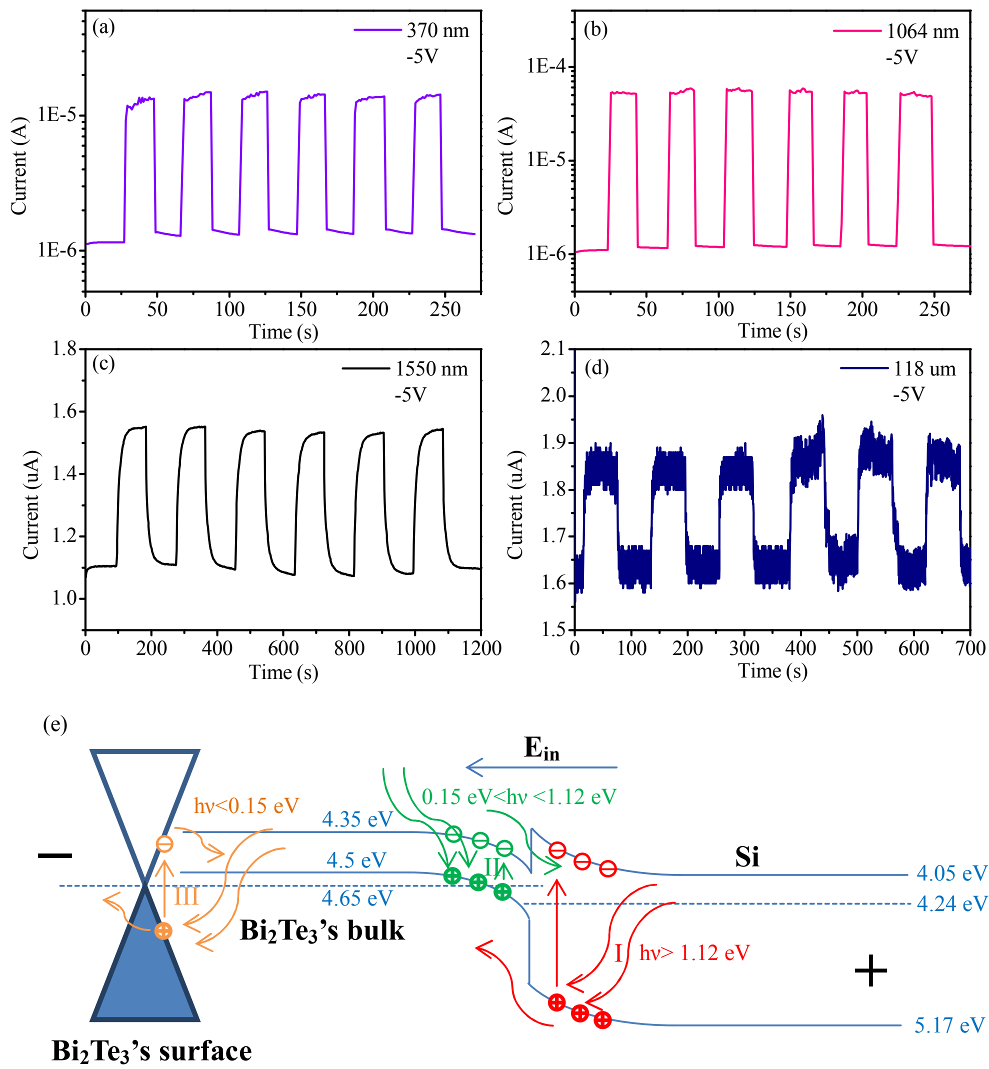

Nanoscale Accepted Manuscript

Figure 4.

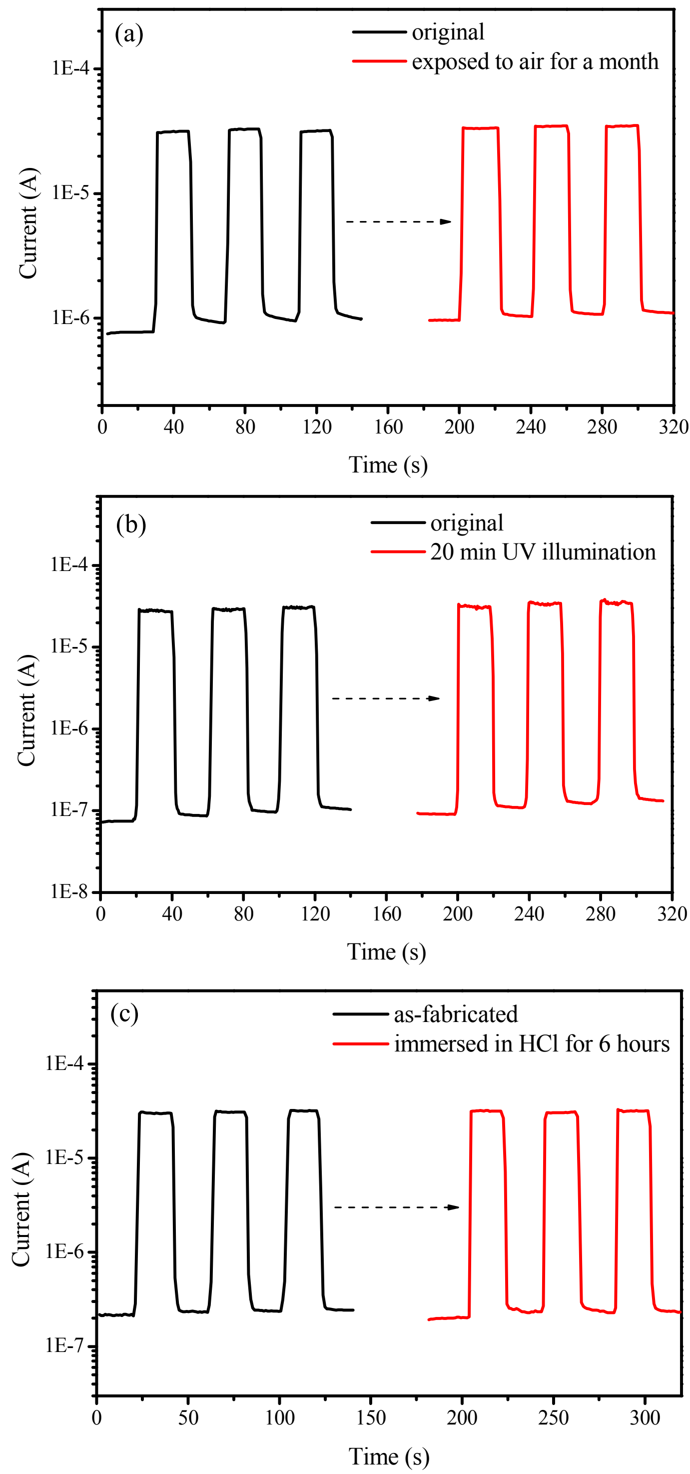

Nanoscale Accepted Manuscript